POLITECNICO
MILANO 1863

SCUOLA DI INGEGNERIA INDUSTRIALE
E DELL'INFORMAZIONE

Executive Summary of the Thesis

Generalised Conjugate Gradient for the minimisation of energy functionals in deformed nuclei

Laurea Magistrale in Nuclear Engineering - Ingegneria Nucleare

Author: Alessandro Sala

Advisor: Prof. Matteo Passoni

Co-advisor: Prof. Gianluca Colò

Academic year: 2024-2025

1. Introduction

The theoretical study of atomic nuclei provides a bridge between nuclear physics and nuclear engineering. Starting from a framework consistent with quantum mechanics, the strong interaction, and its underlying symmetries, modern nuclear theory aims to construct models characterised by a limited number of free parameters and capable of predicting both nuclear structure and reactions, across a wide range of systems. While experimental data have long provided invaluable insight into nuclear properties and processes, only a coherent theoretical description allows for systematic extrapolations towards regions of the nuclear chart, or physical conditions, that remain beyond current experimental reach. In particular, nuclear fission, despite its crucial importance in nuclear engineering, remains only partially understood from a microscopic standpoint. Current models that use empirical approaches successfully reproduce global quantities like fission barrier heights, fragment mass distributions, and average neutron multiplicities for well studied nuclei. However, these models may rely on a huge number of parameters, which limit their predictive power when extrapolated to systems which are less investigated experimentally. A fully microscopic understanding of the collective dynamics leading from the compound nucleus to scission, the treatment of quantum many-body correlations, and the description of fragment excitation and emission remain among the major open challenges, particularly relevant for the simulation of next-generation reactors, which require the accurate description of nuclei and fuel materials – far less explored than those employed in traditional thermal systems – to be correctly predicted.

1.1. Microscopic description of nuclei

In this regard, the approach to the microscopic description of nuclei, is the one of the many-body theory, which starting from the interacting nucleons, aims at building a complete description of the nucleus. The use of phenomenological potentials based on the Woods-Saxon one is still relevant, thanks to its computational feasibility and its capability to include shell effects in a simple manner, but it cannot account for many-body effects. At the moment, there are two competing frameworks that try to tackle the microscopic description of nuclei, (a) the *ab-initio* approach, where the interaction is in principle exact, derived from controlled approxima-

tions of quantum chromodynamics; and (b) the use of effective interactions and nuclear Density Functional Theory.

Ab-initio methods Ab-initio methods, while technically speaking more rigorous, are still limited as of now, since they can only account for light nuclei or medium-heavy nuclei that can be considered as spherical.

Energy density functionals and effective interactions, such as the Skyrme force, on the other hand are more flexible and less computationally expensive, enabling a much wider representation of nuclei across the whole chart, including heavy nuclei and processes such as fission, fusion, reactions and decays, which are of the utmost importance in nuclear engineering.

Density Functional Theory D Vautherin and D M Brink laid the foundations of the nuclear Hartree–Fock theory using the Skyrme interaction in 1972 [5], through spherically symmetric calculations, which are unable to account for nuclear deformations, essential for nuclei far from magic numbers. Over the years, thanks to the increase in computational performance of modern hardware, codes that are able to represent more coordinates have been written. Many of these codes use basis expansions on the harmonic oscillator, which have the downside of not being able to account for nuclei near the drip lines, due to the diffent asymptotic behaviour of the Gaussian basis in the harmonic oscillator and quasi-resonant states [2].

Thanks to the flexibility offered by nuclear DFT, it has been chosen in the present work as the theoretical framework. In particular, using an Energy Density Functional (EDF) built from the Hartree–Fock expectation value of the Skyrme interaction.

2. Objective and methods

The aim of this work is to develop a new implementation of the Hartree–Fock and nuclear DFT methods on an unconstrained 3D mesh, by the use of the Generalised Conjugate Gradient (GCG) algorithm [3].

2.1. Objectives

The goals addressed by this work are the following:

- demonstrate the feasibility of the Generalised Conjugate Gradient for the solution of large-scale eigenvalue problems;
- solve the self-consistent Hartree–Fock equations on an unconstrained 3D mesh;
- verify the numerical accuracy of the new implementation, first against existing spherical codes;
- second against well established deformed codes; and
- attempt to produce original results, and establish the advancement brought to the field by this work.

2.2. Methods

Skyrme Energy Functional A pure HF treatment is not sufficient for a quantitative description of nuclear structure, and a more general energy density functional (EDF) formulation must be adopted. In this work, we employ the Skyrme EDF. This provides the self-consistent single-particle Hamiltonian that forms the basis for the numerical treatment.

Finite Differences and Generalised Conjugate Gradient Once the equations to be solved have been derived, their numerical solution requires both a spatial discretization scheme and an efficient solver for the large-scale eigenvalue problem that arises at each iteration of the self-consistent procedure.

3. Theoretical framework

The energy functional to be minimised is of the form [1]

$$E_{\mathrm{HF}} = \int (\mathcal{E}_{\mathrm{Kin}} + \mathcal{E}_{\mathrm{Skyrme}} + \mathcal{E}_{\mathrm{Coul}}) d\boldsymbol{r}.$$

3.1. Skyrme Functional

The Skyrme functional formulation used is the following [4]:

$$\mathcal{E}_{\mathrm{Skyrme}} = \sum_{t=0,1} \Big\{ C_t^{\rho}[\rho_0]\rho_t^2 + C_t^{\Delta\rho}\rho_t\nabla^2\rho_t + \\ + C_t^{\nabla\cdot J}\rho_t\nabla\cdot\mathbf{J}_t + C_t^{\tau}\rho_t\tau_t \Big\}$$

3.2. Coulomb treatment

Unlike the Skyrme interaction, the Coulomb force is finite-range, giving rise to an unwanted integral operator in the single-particle Hamiltonian. A well known and widely used device is the Slater approximation which gives a local exchange interaction. In this approximation, the Coulomb energy density is given by

$$\mathcal{E}_{\mathrm{Coul}}(\boldsymbol{r}) = \frac{e^2}{2}\left[\int \frac{\rho_p \rho'_p}{|\mathbf{r}-\mathbf{r}'|} d\mathbf{r}' - \frac{3}{2}\left(\frac{3}{\pi}\right)^{\frac{1}{3}} \rho_p^{4/3}\right].$$

The Coulomb potential field is computed from the solution of the Poisson equation associated to the proton charge density. Dirichlet boundary conditions are derived from a quadrupole expansion of the proton charge density.

4. Numerical Implementation

4.1. Finite Differences

Since both the Kohn–Sham (KS) equations consistent with the EDF, and the Poisson equation to solve are linear, we can evaluate them on the chosen mesh, using finite differences to approximate the differential operators. This yields a linear system of the form

$$\sum_{\alpha=1}^{N} A_{\alpha\beta}\varphi_\beta = E\varphi_\alpha$$

for the KS equations, where the shorthand notation $N = 2 \cdot N_x \cdot N_y \cdot N_z$ is used to denote the size of the matrix A, which is $N \times N$. In the case of the Poisson equation, the spin coordinate is not used, so the dimension N is reduced by a factor of 2. In this latter case, the problem has a fixed r.h.s. and reduces to

$$AV_c = \tilde{\rho}_p \tag{1}$$

where $\tilde{\rho}_p$ properly accounts for the boundary conditions.

4.2. Generalised Conjugate Gradient

The GCG method [3] is implemented for the diagonalization of the KS equations. GCG is an iterative eigensolver designed with the aim of improving LOBPCG; it is a blocked algorithm, which uses the inverse power method and previous search directions to generate the subspace in which to search for the eigenvectors of the matrix. The method is implemented with the following modifications:

- it is extended to the complex case, meaning transposition operations are replaced by conjugate transpose operations;
- the blocking on the search vectors is performed with a $[X_{\mathrm{conv}}, X_{\mathrm{act}}]$ scheme, where X_{conv} are the converged vectors, and X_{act} the active vectors;
- the orthonormalization of the column vectors is performed using Gram-Schmidt orthonormalization;
- the problem is simplified in complexity by assuming $B = I$; and
- a diagonal preconditioner is adopted for the CG step.

5. Benchmarks

5.1. Spherical nuclei

The new implementation is shown to be in numerical agreement with the well-established spherical code `hfbcs_qrpa`. Results in table 1 are shown for the light ^{16}O, and in table 2 for the heavier nuclei ^{90}Zr, both calculated neglecting pairing correlations. Unlike radial codes, where the mesh is 1D and its lattice can be made very refined, the unconstrained mesh suffers from the computational cost of a high number of points, as shown by the numerical error when the step size increases in table 2. All spherical calculations use a step size of 0.1 fm.

5.2. Deformed nuclei

The GCG implementation is also validated for deformed nuclei using two different codes. The ground state properties of the light, deformed ^{24}Mg are first compared to the results of the `HFBTHO` code, which is a well-established basis code. After that, a comparison with the more similar Cartesian mesh code `EV8` is shown.

5.3. Basis code and ground state

In table 3, some physical properties of the ground state of ^{24}Mg are compared to the results of the code `HFBTHO`, the results are in accordance and show good agreement. Some differences may arise due to the profoundly different numerical techniques adopted, which may hinder the performance of `HFBTHO` in such a deformed system.
In table 4, the single-particle energy levels of the ground state of ^{24}Mg are shown to demonstrate

Physical quantities

		GCG	`hfbcs_qrpa`
E_{TOT}	[MeV]	-128.402	-128.400
$\langle r_n^2 \rangle^{1/2}$	[fm]	2.6584	2.6585
$\langle r_p^2 \rangle^{1/2}$	[fm]	2.6835	2.6836
$\langle r_{ch}^2 \rangle^{1/2}$	[fm]	2.7805	2.7803

Neutron energy levels

		GCG	`hfbcs_qrpa`
$1s_{1/2}$	[MeV]	-36.140	-36.137
$1p_{3/2}$	[MeV]	-20.611	-20.611
$1p_{1/2}$	[MeV]	-14.427	-14.428

Proton energy levels

		GCG	`hfbcs_qrpa`
$1s_{1/2}$	[MeV]	-32.349	-32.345
$1p_{3/2}$	[MeV]	-17.137	-17.137
$1p_{1/2}$	[MeV]	-11.081	-11.082

Table 1: ^{16}O complete of the Skyrme functional and Coulomb interaction.

the degeneration removal within the same subshell. As predicted by the Nilsson model, levels with a lower $|m_j|$ projection are lowered in energy, while those with a higher projection are raised, with respect to the spherical (degenerate) case.
In figure 1, the ground state density $\rho(x, 0, z)$ of ^{24}Mg is shown. As expected from experimental data, the nucleus is very deformed and prolate.

5.4. Cartesian benchmark and deformation curve

The softness of the ground state with respect to a quadrupole deformation, and the presence of other local minima with energies comparable to the one showed by the axial configuration in figure 1, may be verified by plotting the deformation curve. It is computed by imposing a quadrupole constraint on the total density. Additionaly, in our framework, we must constrain the nucleus centre of mass in the origin, as to prevent spourious contributions to the $\langle \mathcal{Q}_{20} \rangle$ value, and impose axial symmetry by constraining

$$\langle \mathrm{Re}\, \mathcal{Q}_{22} \rangle = \langle \mathrm{Im}\, \mathcal{Q}_{22} \rangle = 0.$$

The comparison of the two deformation curves is shown in figure 2. The two codes show excellent agreement, with similar energies and ground state quadrupole moment. The difference in the rightmost part of the figure may be attributed to different numerical methods used by the two codes, both in the calculation of the discretized derivatives and the minimisation of the energy functional. The quadrupole moment relates to the β_2 deformation parameter as

$$\beta_2 = \frac{4\pi \langle \mathcal{Q}_{22} \rangle}{3AR^2}.$$

This formulation is used throughout the implementation of this work.

Physical quantities

		GCG	`hfbcs_qrpa`
E_{TOT}	[MeV]	-783.587	-783.325
$\langle r_n^2 \rangle^{1/2}$	[fm]	4.2854	4.2872
$\langle r_p^2 \rangle^{1/2}$	[fm]	4.2196	4.2212
$\langle r_{ch}^2 \rangle^{1/2}$	[fm]	4.2767	4.2704

Table 2: ^{90}Zr, box size [-15,+15] fm, step size 0.43 fm.

		GCG	`HFBTHO`
E_{TOT}	[MeV]	-197.219	-197.030
$\langle r_n^2 \rangle^{1/2}$	[fm]	2.9998	2.9996
$\langle r_p^2 \rangle^{1/2}$	[fm]	3.0346	3.0326
$\langle r_{ch}^2 \rangle^{1/2}$	[fm]	3.1240	3.4614
$\langle \mathcal{Q}_{20} \rangle$	[-]	33.905	33.881

Table 3: Results for ^{24}Mg ground state, no pairing interaction, box $[-10, +10]$ fm, step size 0.33 fm, SkM* parametrisation.

6. Original results

Since the benchmarks show a correct implementation, both of the theoretical framework and the numerical methods, we attempted to produce some original results.

6.1. ^{20}Ne clustering

The formation of clusters in light nuclei has been a research focus object in recent years. The in-

Shell	$\|m_j\|$	E [MeV]
$1s_{1/2}$	1/2	-39.281
$1p_{3/2}$	1/2	-28.381
$1p_{3/2}$	3/2	-24.224
$1p_{1/2}$	1/2	-18.680
$1d_{5/2}$	1/2	-16.743
$1d_{5/2}$	3/2	-14.130

Table 4: Single-particle energy levels in the ground state of ^{24}Mg.

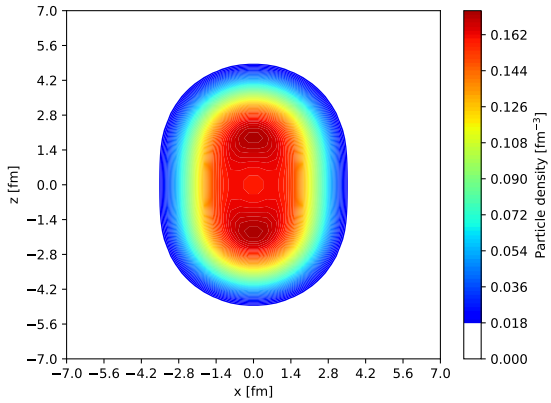

Figure 1: ^{24}Mg ground state density $\rho(x, 0, z)$, calculation done on a box $[-10, +10]$ fm, step size 0.33 fm, SkM* parametrisation.

terest stems from different reasons. The formation of clusters at low density is a strong indicator of specific correlations (n-p correlations or alpha-particle, ie 'quartetting' correlations) and a strong test for theory. At the same time, clustering may have impact on reactions and astrophysical processes. It has to be noted that cluster formation during fission has been highlighted. This phenomena is studied using the Nucleon Localization Function (NLF), which is the conditional probability of finding another nucleon, if one is present in $\boldsymbol{r}$, and it reads

$$C_q(\boldsymbol{r}) = \left[1 + \left(\frac{\tau_q\rho_q - \frac{1}{4}|\nabla\rho_q|^2}{\rho_q\tau_q^{\mathrm{TF}}}\right)^2\right]^{-1}.$$

In figure 3, we show that the ground state of ^{20}Ne displays prominent clusters on top and bottom of a central core. This happens consistently for different Skyrme functionals.

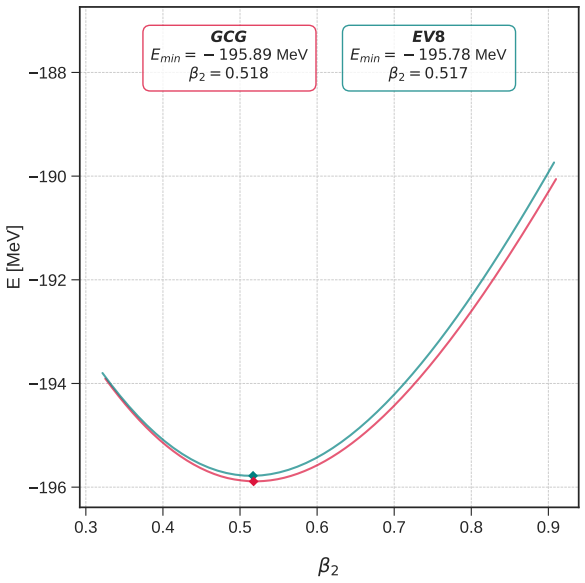

Figure 2: Comparison with the `EV8` code for ^{24}Mg, no pairing interaction, box $[-10, +10]$ fm, step size 0.6 fm, SLy4 parametrisation.

6.2. Near-drip line nuclei

Since a Cartesian mesh is well-suited for the study of weakly bound systems, we present the study of two nuclei near the drip lines. In this section, results regarding the two deformed nuclei ^{42}Si and ^{28}S are presented, the former being a neutron-rich nucleus, the latter being a proton-rich nucleus. Being weakly bound systems, taking direct measurements of quantities like radii, deformations through spectroscopy etc, is not yet possible.

We compare the experimental neutron S_n or proton S_p separation energy with the theoretical value calculated using Koopmans' theorem. In table 6, we show that both the SLy4 and SkM* functionals give results similar to experimentally measured values.

		SLy4	SkM*	Exp.
E	[MeV]	-313.13	-320.76	-317.16
S_n	[MeV]	4.349	4.990	4.458
$\langle r_n^2\rangle^{1/2}$	[fm]	3.716	3.705	-
$\langle r_p^2\rangle^{1/2}$	[fm]	3.294	3.276	-
$\langle r_{ch}^2\rangle^{1/2}$	[fm]	3.380	3.362	-
β_2	[-]	-0.332	0.313	-

Table 5: Results for ^{42}Si, box $[-11, +11]$ fm, step size 0.37 fm.

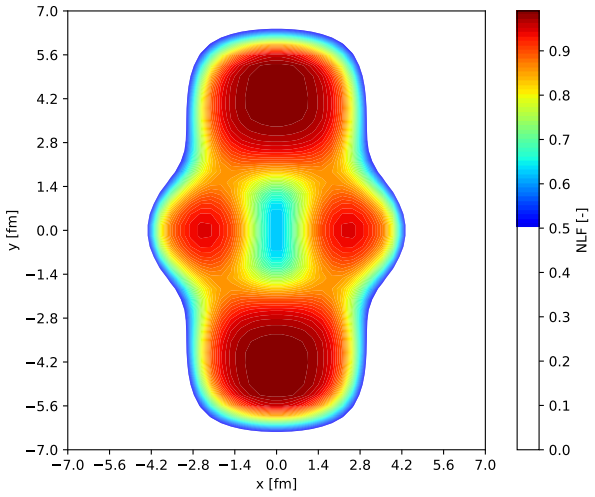

Figure 3: NLF, KDE33 functional.

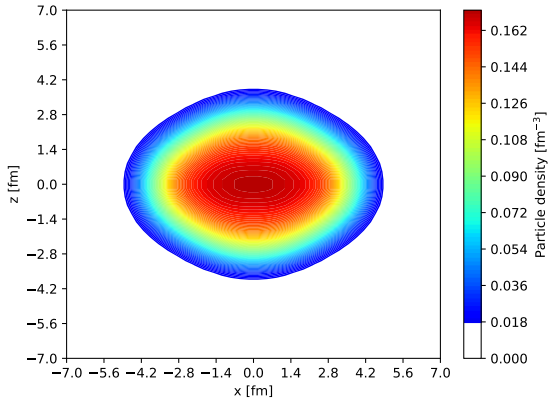

Figure 4: ^{42}Si density $\rho(x, 0, z)$, calculation done on a box $[-11, +11]$ fm.

7. Conclusions

We showed that the implementation of a Cartesian mesh code, that is able to solve the minimisation of energy functionals, even for deformed nuclei, is both possible and efficient when using the Generalised Conjugate Gradient method. The results obtained with the GCG implementation are in good agreement with the results obtained with the well-established spherical code `hfbcs_qrpa` and the deformed codes `EV8` and `HFBTHO`. Thanks to the flexibility offered by the method, many further advancements based on this work can be carried out. Most notably, the implementation of a full Hartree–Fock–Bogoliubov approach, which would allow the self-consistent treatment of the mean-field and pairing interactions. On top of that, a similar approach can be used to solve other analogous problems in nuclear physics, such as in the ab-initio methods.

		SLy4	SkM*	Exp.
E	[MeV]	-209.69	-211.64	-209.41
S_n	[MeV]	3.370	3.330	2.556
$\langle r_n^2 \rangle^{1/2}$	[fm]	3.013	2.997	-
$\langle r_p^2 \rangle^{1/2}$	[fm]	3.235	3.225	-
$\langle r_{ch}^2 \rangle^{1/2}$	[fm]	3.318	3.308	-
β_2	[-]	0.314	0.289	-

Table 6: Results for ^{28}S, box $[-10, +10]$ fm, step size 0.34 fm.

References

[1] M. Bender, P.-H. Heenen, and P.-G. Reinhard. Self-consistent mean-field models for nuclear structure. *Reviews of Modern Physics*, 75(1):121–180, 2003.

[2] G. Colò. Nuclear density functional theory. *Advances in Physics: X*, 5(1):1740061, 2020.

[3] Yu Li, Hehu Xie, Ran Xu, Chun'guang You, and Ning Zhang. A parallel generalised conjugate gradient method for large scale eigenvalue problems. *CCF Transactions on High Performance Computing*, 2(2):111–122, jun 2020. The corresponding computing package can be downloaded from the web site: `https://github.com/pase2017/GCGE-1.0`.

[4] P.D. Stevenson and M.C. Barton. Low-energy heavy-ion reactions and the skyrme effective interaction. *Progress in Particle and Nuclear Physics*, 104:142–164, 2019.

[5] D. Vautherin and D. M. Brink. Hartree–fock calculations with skyrme's interaction. i. spherical nuclei. *Phys. Rev. C*, 5:626–647, Mar 1972.